European Radiology (2019) 29:4096–4104
https://doi.org/10.1007/s00330-018-5964-3

NEURO

Amide proton transfer–weighted MRI can detect tissue acidosis and monitor recovery in a transient middle cerebral artery occlusion model compared with a permanent occlusion model in rats

Ji Eun Park[1] · Seung Chai Jung[1] · Ho Sung Kim[1] · Ji-Yeon Suh[2] · Jin Hee Baek[3] · Chul-Woong Woo[2] · Bumwoo Park[1] · Dong-Cheol Woo[2]

Received: 8 August 2018 / Revised: 30 November 2018 / Accepted: 7 December 2018 / Published online: 21 January 2019

Abstract

Objectives To assess whether increases in amide proton transfer (APT)–weighted signal reflect the effects of tissue recovery from acidosis using transient rat middle cerebral artery occlusion (MCAO) models, compared to permanent occlusion models.

Materials and methods Twenty-four rats with MCAO (17 transient and seven permanent occlusions) were prepared. APT-weighted signal (APTw), apparent diffusion coefficient (ADC), cerebral blood flow (CBF), and MR spectroscopy were evaluated at three stages in each group (occlusion, reperfusion/1 h post-occlusion, and 3 h post-reperfusion/4 h post-occlusion). Deficit areas showing 30% reduction to the contralateral side were measured. Temporal changes were compared with repeated measures of analysis of variance. Relationship between APTw and lactate concentration was calculated.

Results Both APTw and CBF values increased and APTw deficit area reduced at reperfusion (largest $p = .002$) in transient occlusion models, but this was not demonstrated in permanent occlusion. No significant temporal change was demonstrated with ADC at reperfusion. APTw deficit area was between ADC and CBF deficit areas in transient occlusion model. APTw correlated with lactate concentration at occlusion ($r = -0.49$, $p = .04$) and reperfusion ($r = -0.32$, $p = .02$).

Conclusions APTw values increased after reperfusion and correlated with lactate content, which suggests that APT-weighted MRI could become a useful imaging technique to reflect tissue acidosis and its reversal.

Key Points

- *APT-weighted signal increases in the tissue reperfusion, while remains stable in the permanent occlusion.*
- *APTw deficit area was between ADC and CBF deficit areas in transient occlusion model, possibly demonstrating metabolic penumbra.*
- *APTw correlated with lactate concentration during ischemia and reperfusion, indicating tissue acidosis.*

Keywords Acidosis · Reperfusion · Amides · Magnetic resonance imaging

Ji Eun Park and Seung Chai Jung contributed equally to this work.

Electronic supplementary material The online version of this article (https://doi.org/10.1007/s00330-018-5964-3) contains supplementary material, which is available to authorized users.

✉ Ho Sung Kim
radhskim@gmail.com

[1] Department of Radiology and Research Institute of Radiology, University of Ulsan College of Medicine, Asan Medical Center, 43 Olympic-ro 88, Songpa-Gu, Seoul 05505, South Korea

[2] Asan Institute for Life Sciences, Asan Medical Center, Seoul 05505, South Korea

[3] University of Ulsan College of Medicine, Asan Medical Center, Seoul 05505, South Korea

Abbreviations

ADC	Apparent diffusion coefficient
APTw	Amide proton transfer–weighted signal
CBF	Cerebral blood flow
MCAO	Middle cerebral artery occlusion

Introduction

The pH of the brain is approximately 7.2 under normal conditions, but decreases during ischemia [1], when glucose is anaerobically metabolized. The introduction of amide proton transfer (APT)–weighted magnetic resonance imaging (MRI) [2, 3] has enabled assessment of tissue acidosis in ischemia, as

the APT-weighted voxel values are reduced in regions of tissue acidosis. After ischemic insult, the APT-weighted signals change, as pH affects the exchange rate of amide protons [2–4], while protein content and temperature in the brain remain unchanged [2, 5]. In acute ischemic tissue, changes in pH and APT-weighted signaling have been shown to occur before changes in diffusion-weighted imaging (DWI) indicative of cytotoxic edema [4, 6]. Moreover, APT-weighted MRI may aid in defining penumbral tissue [4, 7, 8], where areas of APT deficit are intermediate in size between areas of apparent diffusion coefficient (ADC) and perfusion deficits.

Although APT-weighted MRI has been studied in ischemic tissue [2, 3, 9–12], few studies to date have examined its use in reperfused tissue, where metabolism switches from anaerobic to aerobic and the pH returns to its normal physiological level. DWI or perfusion-weighted imaging (PWI) techniques such as arterial spin labeling (ASL) or dynamic susceptibility contrast imaging are often used to assess the state of tissue following reperfusion [13, 14]. However, ischemia-related changes in ADC values may reverse after reperfusion, in contrast to the assumed equivalence with diffusion-restriction lesions in the infarct core [15, 16]. Although perfusion-weighted MRI is useful for assessing the direct perfusion dynamics of tissue, perfusion is also reduced in benign oligemias [13], suggesting that perfusion-weighted MRI results do not reflect tissue metabolism. Regional variations in oxygen influx can result in the metabolic heterogeneity of reperfused tissue, as well as spatial variations in the normalization of pH [17]. Thus, APT-weighted MRI may provide complementary information to assess the state of tissue after reperfusion.

We hypothesized that increases in APT-weighted image intensity would reflect the state of tissue recovery from acidosis, and that they would provide complementary information to ADC, cerebral blood flow (CBF), and lactate content measurements. Incorporating APT-weighted MRI into a multiparametric MR approach has been demonstrated in humans with permanent stroke [18] and in rat stroke models [14], but has not been performed in the post-reperfusion state. This study therefore assessed whether increases in APT-weighted signaling reflect the effects of tissue recovery from acidosis by comparing the values of transient rat middle cerebral artery occlusion (MCAO) models with those of permanent occlusion models.

Materials and methods

Animal model

This study was approved by the Institutional Animal Care and Use Committee of Asan Medical Center. All experimental procedures were carried out in strict accordance with the Association for Assessment and Accreditation of Laboratory Animal Care. All animal experiments described below have been reported in compliance with the ARRIVE (Animal Research: Reporting in Vivo Experiments) guidelines [19]. Transient MCAO was induced in 24 adult (9 to 10 weeks) male Wistar rats weighing 280–330 g (mean ± standard deviation, 300.3 ± 23 g). For MCAO surgery, the rats were anesthetized with 1.5% isoflurane in 70% N_2O/30% O_2 (flow rate, 1.0 L/min), and the right MCA was occluded by inserting a 4-0 silk suture coated with a commercial silicon rubber–coated 5-0 nylon monofilament (tip diameter, 0.35–0.37 mm) into the lumen of the internal carotid artery to block the origin of the MCA. Reperfusion was performed 1 h after initial occlusion. MRI data were acquired at occlusion, immediately after reperfusion (1 h post-occlusion), and at 3 h post-reperfusion (4 h post-occlusion). During MRI acquisitions, isoflurane anesthesia was halted and replaced by a loading bolus of 20 mg/kg alpha-chloralose and 1.0 mg/kg pancuronium, followed by continuous infusion of alpha-chloralose (up to 30 mg/kg/h) with pancuronium (up to 1.25 mg/kg/h). Respiratory rates during MRI were monitored using a small-animal monitoring and gating system (SA Instruments, Inc.). After the last follow-up, the rats were immediately sacrificed and specimens were subjected to 2,3,5-triphenyltetrazolium hydrochloride staining.

Permanent MCAO was induced in another group of seven adult male Wistar rats. The occlusion surgery, experimental conditions, imaging protocols, and data analysis were identical to those in rats that underwent reperfusion. The average intervals between time points were 76.0 ± 7.6 min and 205.0 ± 30.8 min for the reperfusion group and 80.1 ± 19.6 min and 211.6 ± 51.7 min for the permanent group.

Samples were stained with 2,3,5-triphenyltetrazolium hydrochloride after the last follow-up. Five 2-mm-thick slices were sectioned coronally and incubated in 2% 2,3,5-triphenyltetrazolium hydrochloride at 37 °C for 30 min. Brain slices were photographed using a digital camera. The stained regions were defined as normal and the unstained regions as infarcted lesions [20].

Multimodal MRI data acquisition and preprocessing

Rats were placed in a dedicated holder and positioned in the isocenter of a 7.0-T MRI scanner (Bruker Biospin) equipped with a 40-cm bore, a 660 mT/m gradient, and shim systems. High-order FASTMAP shimming and cross coils (volume-coil excitation, surface-coil detection) with active decoupling were used to achieve a homogeneous magnetic field. The multimodal MRI protocols included T2-weighted imaging, DWI, ASL, APT-weighted MRI, and ^{1}H-MR spectroscopy. For MR spectroscopy, FASTMAP shimming was applied to achieve a homogeneous B_0 and B_1 magnetic field on the MR console, and MR spectroscopy was obtained when the full width at a half maximum at the unsuppressed water resonance

is less than 5 Hz. As APTw contrast is highly sensitive to local B_0 and B_1variations, B_0 and B_1 corrections were applied according to previously established methods [21]. The detailed protocol descriptions and B_0 and B_1 corrections methods are in Supplementary Materials.

Magnetization transfer ratio (MTR) asymmetry analysis was used to calculate the signal from the amide protons reflected by water [22]. Maps of the asymmetric APT ratio (APT-weighted voxel values), APTw (+ 3.5 ppm) = MTR (− 3.5 ppm) − MTR (+ 3.5 ppm), were calculated based on B_0 point-by-point corrected interpolated images, S[− 3.5 ppm] and S[+ 3.5 ppm] [23].

Imaging analysis

To compare multiparametric MRI data from the same location, the three-dimensional (3D) DWI and a single slice of the ADC, CBF, and APTw maps were co-registered, and a mask chosen on the basis of the highest *b*-value in the diffusion images was used to remove background and extracranial signals. The images were registered to the brain-extracted DWI volume using an affine transformation with 12 degrees of freedom, tri-linear interpolation, and a normalized mutual information cost function [24]. MRI data were preprocessed using AFNI software (http://afni.nimh.nih.gov/afni) [25] by a researcher with 3 years of experience in image analysis.

Assessment of area of deficit First, a region of interest (ROI) denoting the CBF perfusion deficit area was manually drawn by two stroke neuroradiologists, with 15 and 4 years of experience in neuroradiology, working in consensus using ImageJ software (https://imagej.nih.gov/ij/). Before calculation, a ROI mask (200 mm^2) was manually drawn on each rat's normal side, and the averaged ADC, CBF, and APTw values were obtained for this region. The same ROI mask was applied as regional variations exist in the normal rat brain in magnetization transfer [26], which might affect the area of APTw deficit after threshold was applied. Thresholds for areas of ADC, CBF, and APTw deficit were defined as 30% reductions compared with the values on the normal contralateral side. Thresholds were used to define perfusion deficit areas, as these areas enclosed both diffusion-restriction and pH deficit areas [4]. The 30% threshold was chosen because a 30% ± 2% reduction (or 0.53 ± 0.03 $\mu m^2/s$) had previously been shown to be a viable and robust threshold for ADC [27]. As there is no previously determined threshold for APTw, the 30% reduction criterion was therefore also adopted in this exploratory analysis. The deficit areas were determined using a semi-automatic thresholding method developed with in-house software written in MATLAB 2014b (The MathWorks). An example of this thresholding method is shown in Fig. 1.

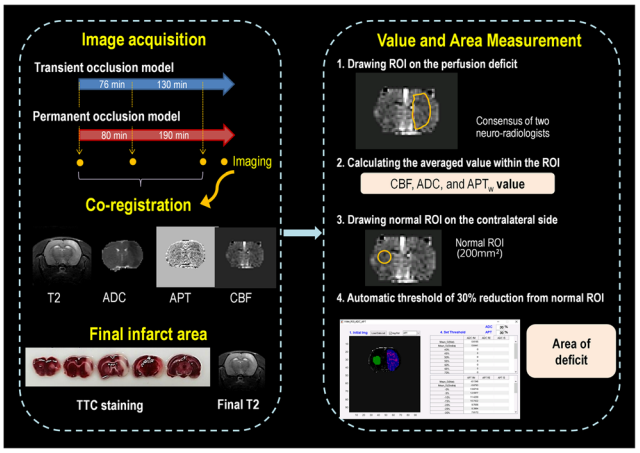

Fig. 1 The analysis pipeline. After image acquisition, a co-registration process was performed between T2-weighted imaging, and apparent diffusion coefficient (ADC), amide proton transfer (APT), and cerebral blood flow (CBF) maps. The final infarct volume was assessed using the final diffusion-weighted imaging and 2,3,5-triphenyltetrazolium hydrochloride (TTC) staining. CBF, ADC, and APTw values were calculated according to the CBF deficit drawn by the two neuroradiologists. The area of deficit was automatically calculated by a threshold algorithm for ADC and APTw values within the CBF deficit area

Assessment of final infarct area Final infarct areas were determined by drawing ROIs on the final T2-weighted images, which were then co-registered with photographs of the TTC-stained brain slices using imaging analysis software (ImageJ). ROIs were drawn by the two abovementioned stroke neuroradiologists working in consensus. All brain slices were 3 mm thick.

Statistical analysis

The characteristics of the transient and permanent occlusion models were compared using Mann-Whitney *U* tests. MRI parameters were initially assessed for normality using the Shapiro-Wilk test. The MRI parameters were found to be normal and were expressed as mean ± standard deviation. The MR parameters were compared using repeated-measures analysis of variance (ANOVA; a paired analysis that tests if the mean of the differences between each pair of measurements is zero), where the between-subjects factor was "subject group" and the within-subjects factor was "temporal change" across the three serial acquisitions. When differences were found between groups, post hoc analyses were conducted with Bonferroni corrections applied for multiple comparisons.

The relationships of APTw values with lactate concentrations and normalized lactate peaks were assessed using the Pearson correlation coefficient. A p value < .05 was considered statistically significant. All statistical analyses were performed using the MedCalc 15.6.1 software package (MedCalc Software) and R version R 3.3.3 (R Foundation for Statistical Computing; http://www.R-project.org, 2016).

Results

There were no statistically significant differences in weight and imaging intervals between rats in the transient and permanent occlusion groups (Table 1). Infarct areas were significantly larger in the permanent than in the transient occlusion group ($p < .001$).

Comparisons of the transient and permanent occlusion groups

Table 2 summarizes the results for the transient and permanent occlusion groups, with the results of post hoc analyses shown in Supplementary Table 1.

In the transient occlusion group (Fig. 2), both APTw ($p = .002$) and CBF ($p = .001$) significantly increased from the occlusion to the reperfusion stage, whereas there was no significant temporal change ($p > .05$) in ADC. ^{1}H-MRS showed no temporal changes in lactate concentration and lactate/(Cho+Cr) ($p > .05$), whereas a significant temporal decrease was observed in total choline concentration ($p < .001$).

In the permanent occlusion group (Fig. 3), no significant temporal changes were observed in APTw, CBF, and ADC ($p > .05$). From 1 to 4 h post-occlusion, both lactate concentration ($p < .001$) and lactate/(Cho+Cr) ($p = .001$) increased significantly, whereas total choline concentration decreased significantly ($p = .002$) from occlusion to 4 h post-occlusion.

Comparisons of the temporal changes in MR parameters revealed that CBF ($p < .001$), APTw ($p = .006$), and ADC ($p = .008$) differed significantly in the transient and permanent occlusion groups. However, no significant between-group differences were observed in ^{1}H-MRS values. The averaged APTw, CBF, and ADC values in normal contralateral brains were $-5.8\% \pm 1.7\%$, 1.8 ± 0.4 mL/g/min, and 0.7 ± 0.0 μm^2/ms, respectively, and did not differ significantly between the two groups.

Deficit areas in the transient and permanent occlusion groups

Table 3 summarizes the extent of the areas of deficit in the transient and permanent occlusion groups, as well as showing the results of post hoc analysis. In the transient occlusion group, the APTw deficit area decreased after reperfusion, especially in the reperfusion state ($p = .023$). The CBF deficit area decreased over the three stages, with significant increases seen from reperfusion to 3 h post-reperfusion (largest, $p = .023$). However, the ADC deficit area did not change significantly after reperfusion ($p > .05$).

In the permanent occlusion group, the APT_{asym} deficit area did not change significantly over the three stages ($p > .05$). The CBF deficit area increased significantly only from 1 to 4 h post-occlusion ($p = .03$). The ADC deficit area increased over the three stages ($p = .002$), with the difference between the occlusion and 4 h post-occlusion stages being statistically significant ($p = .015$). CBF ($p = .011$) and ADC ($p = .003$) deficits differed significantly in the two groups.

Temporal changes in the deficit areas are shown in Fig. 4. The deficit areas were compared among the multiparametric MRI in each individual. During ischemia, the APTw deficit area was larger than the ADC deficit area in all subjects. In the transient occlusion group, the APTw deficit areas were generally intermediate to the ADC and CBF deficit areas, except in two rats during reperfusion and in five rats at 3 h post-reperfusion. In the permanent occlusion group, the APTw deficit areas were consistently smaller than the CBF deficit areas over the three time points, but overlapped with the ADC deficit areas in three of seven rats at 1 and 4 h post-occlusion.

Correlations between APT-weighted signals and lactate content during ischemia and reperfusion

APT-weighted signals were correlated with lactate content during ischemia (including the occlusion states of both the transient and permanent occlusion models) and reperfusion (including reperfusion and 3 h post-reperfusion in the transient occlusion model). APTw correlated negatively with lactate content during ischemia ($r = -0.49$, $p = .04$) and after reperfusion ($r = -0.32$, $p = .02$). Neither total choline nor the normalized lactate peak showed a significant correlation with APTw, in either the transient or permanent occlusion groups.

Table 1 Characteristics of the transient and permanent occlusion models

	Transient occlusion	Permanent occlusion	*p* value*
Number of rats	17	7	
Weight (g)	297.6 ± 16.2	300.3 ± 27.1	.92
Time to reperfusion (min)	76 ± 5.7	NA	
Imaging interval (min)			
First to second imaging	76.0 ± 7.6	80.7 ± 19.6	.89
First to third imaging	205.8 ± 30.8	272.0 ± 31.5	.11
Final infarct area (mm^2)	15.3 ± 7.1	39.7 ± 6.5	< .001

Data are expressed as median ± interquartile range. *By the Mann-Whitney *U* test (after a normality test)

Table 2 Multiparametric MRI values for the transient and permanent occlusion groups

	Transient occlusion group				Permanent occlusion group				$p^{\dagger}$
	Occlusion	Reperfusion	3 h post-reperfusion	p*	Occlusion	1 h post-occlusion	4 h post-occlusion	p*	
CBF (mL/g per min)	1.0 ± 0.1	2.6 ± 0.1	2.1 ± 0.7	.002**	0.9 ± 0.2	0.8 ± 0.3	0.7 ± 0.1	.24	< .001**
APTw (%)	−7.7 ± 1.8	−6.5 ± 1.3	−5.7 ± 1.5	.001**	−7.7 ± 1.2	−8.6 ± 1.0	−8.0 ± 0.7	.18	.006**
ADC (μm^2/ms)	0.54 ± 0.06	0.53 ± 0.06	0.54 ± 0.09	.92	0.49 ± 0.03	0.45 ± 0.03	0.45 ± 0.04	.20	.008**
Lactate (mM)	11.7 ± 6.1	11.4 ± 8.0	9.3 ± 7.5	.27	11.1 ± 4.4	11.5 ± 3.0	18.4 ± 2.6	.001**	.28
Total choline (mM)	1.2 ± 0.2	1.0 ± 0.1	0.7 ± 0.2	< .001**	1.1 ± 0.1	0.9 ± 0.1	0.9 ± 0.1	.004**	.925
Lactate/(Cho+Cr)	1.6 ± 0.8	1.9 ± 1.3	2.3 ± 1.9	.27	1.6 ± 0.7	1.8 ± 0.4	3.6 ± 0.8	< .001**	.427

The results of post hoc analysis are shown in Supplementary Table 1. All values are expressed as mean ± standard deviation. *Significance of temporal changes in each parameter for three serial sequences (within-subject factor). **$p < 0.5$. † Significance of between-group differences in temporal changes (between-subject factor). Total choline represents the sum of glycerophosphocholine + phosphocholine (GPC + PCh)

ADC apparent diffusion coefficient, *APTw* amide proton transfer–weighted voxel values, *CBF* cerebral blood flow

Supplementary Table 2 summarizes the correlations between APT and MR spectroscopy parameters.

Discussion

Our results showed that APTw values increased significantly and APTw deficit areas decreased significantly immediately after reperfusion, suggesting that APT-weighted MRI can reflect tissue recovery. By contrast, there were no significant temporal changes in APTw, CBF, and ADC values in the permanent occlusion model. APTw values correlated negatively with lactate concentration, further indicating that APT-weighted MRI is a pH-weighted imaging technology that can show reversals in tissue metabolism and ischemia after reperfusion therapy. These findings indicate that APT-weighted MRI provides useful information reflecting tissue acidosis and its reversal, suggesting that this method may be particularly useful when assessing patients after reperfusion therapy, and could be translated into clinical practice.

After ischemic insult, APTw decreases because metabolism is sustained by anaerobic glycolysis [3, 4, 28], with the resulting lactic acid reducing pH [29, 30]. Conversely, APTw is expected to increase after reperfusion, although this had not previously been measured by APT-weighted MRI. A preliminary study showed that APTw gradually recovered in a transient MCAO model [31], but the imaging intervals were 1, 3, and 7 days, limiting the evaluation of early temporal changes. Another APT-weighted MRI study was performed using a transient rat MCAO model, but because APT was not determined at baseline occlusion [14], that study could not assess temporal changes after reperfusion. The present study showed that the APTw value and deficit area recovered immediately after filament removal, with the correlation between APTw values and lactate concentrations suggesting that APT-weighted MRI reflected an increase in pH and an alleviation of anaerobic metabolism.

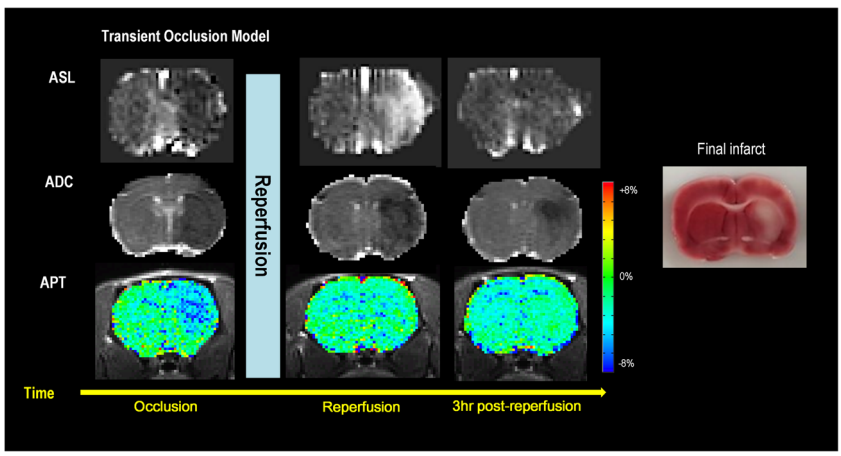

Fig. 2 Illustration of the transient occlusion model. Reperfusion was successful with increased perfusion immediately after reperfusion. Temporal reversal of both values and areas of deficit in apparent diffusion coefficients and amide proton transfer–weighted MRI was observed, especially immediately after reperfusion

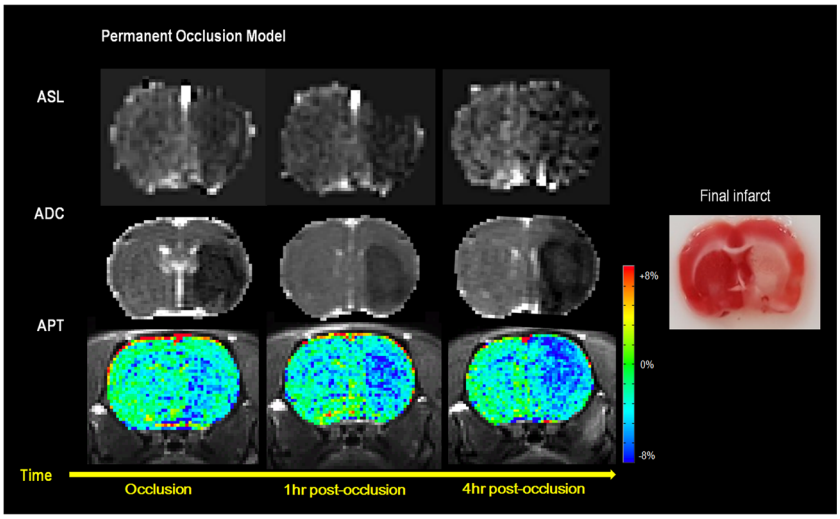

Fig. 3 Illustrative case of the permanent occlusion model. No significant temporal recovery in value was observed, along with increases in the deficit areas in the apparent diffusion coefficient, amide proton transfer–weighted MRI, and cerebral blood flow maps

A comparative analysis of the transient and permanent occlusion models showed that incorporating APT-weighted MRI into a multiparametric MR approach could help determining the success of reperfusion. The decrease in CBF at the occlusion stage was about 50–55% compared with the contralateral side, in accordance with CBF viability thresholds from previous MCAO studies [27, 32]. Following reperfusion, both APTw and the APT deficit area reversed significantly in the transient, but not in the permanent, occlusion model. The CBF value markedly increased, and the CBF deficit area decreased, but excessive hyperperfusion may lead to reperfusion injury [33]. Biophysical information obtained with APT-weighted MRI may therefore predict enhanced recovery in the subacute stage [28]. APT-weighted MRI has been shown to provide biophysical information [34] in rat models [14] and humans [18] with permanent occlusion, with less profound metabolic disturbances expected with higher APT signal. This hypothesis was confirmed by the experimental data from the transient occlusion model in the present study.

The areas of APT deficit were intermediate in size relative to the areas of ADC and perfusion deficit in all rats during ischemia and most during transient occlusion. This sizeable mismatch with CBF and ADC maps was observed in previous studies, which suggested that APT-weighted MRI reflected the outer boundaries of a metabolic penumbra [4]. Our results are in agreement with the concept that MRI data in stroke are inherently complementary to biophysical information [35], as regional metabolism can be heterogeneous [36] and difficult to assess using a single imaging parameter. Also, we adopted a robust automatic measurement using a 30% threshold to obtain areas of ADC and APT_{asym} deficits, finding that the areas of APT deficit gradually decreased after reperfusion. These findings are in agreement with suggestions that APT-weighted MRI could be used to complement commonly used PWI and/or DWI imaging [4, 7], as APT-weighted MRI provides information on tissue acidosis, as well as changes in both values and affected areas before and after reperfusion therapy.

Table 3 Deficit areas on multiparametric MRI in the transient and permanent occlusion groups

	1	2	3	p*	p value for post hoc analysis‡		
Transient occlusion ($n = 17$)	Occlusion	Reperfusion	3 h post-reperfusion		1 vs 2	2 vs 3	1 vs 3
Area of CBF deficit (mm^2)	25.2 ± 7.9	21.8 ± 9.8	16.6 ± 8.0	< .001**	.07	.002**	< .001**
Area of APT deficit (mm^2)	22.1 ± 8.1	15.9 ± 5.9	11.8 ± 5.4	< .001**	.023**	.118	.002**
Area of ADC deficit (mm^2)	10.6 ± 6.2	7.3 ± 7.2	10.9 ± 10.6	.249	.482	.162	1
Permanent occlusion ($n = 7$)	Occlusion	1 h post-occlusion	4 h post-occlusion				
Area of CBF deficit (mm^2)	29.2 ± 2.9	27.5 ± 6.0	34.4 ± 4.3	.03**	1	.163	.027**
Area of APT deficit (mm^2)	18.3 ± 4.6	14.5 ± 4.7	17.3 ± 8.3	.623	.643	1	1
Area of ADC deficit (mm^2)	11.3 ± 3.9	18.0 ± 4.3	25.1 ± 6.7	.002**	.185	.131	.015**

All values are expressed as mean ± standard deviation. *Significance of temporal change in each parameter for three serial sequences. **$p < 0.5$. ‡ Bonferroni-corrected p value

ADC apparent diffusion coefficient, *APT* amide proton transfer, *CBF* cerebral blood flow

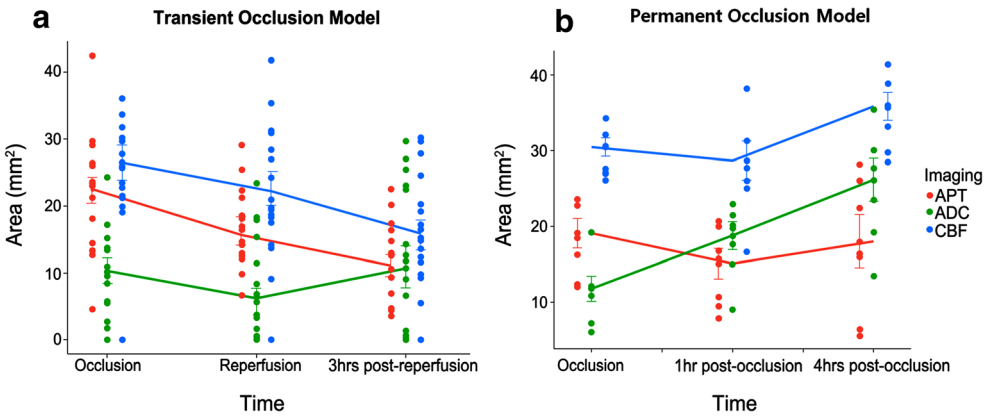

Fig. 4 Comparative temporal changes in the deficit areas of the transient and permanent occlusion models. **a** In the transient occlusion model, areas of APTw and CBF deficit gradually decreased. In most rats, areas of APTw deficit were larger than areas of ADC deficit, but smaller than areas of CBF deficit. **b** In the permanent occlusion model, CBF deficit areas were consistently larger than APTw deficit areas

Of note, our failure to find a significant change in ADC after reperfusion is different from previous studies that ADC values recovered [37–39] and even overshot in reperfused previously ischemic regions [38]. This lack of significant change might be due to the ADC deficit area being calculated within the perfusion deficit area, not over the entire affected hemisphere. As the CBF perfusion deficit decreased after reperfusion, the ADC deficit area was also reduced, and the ADC value within it more closely represented the infarct core. Future studies with a more robust threshold for CBF deficit and subsequent definition of ADC deficit are needed.

This study had several limitations, including the small number of study subjects. In addition, final infarcts were assessed at 3 h post-reperfusion, in contrast to the commonly used long-term tissue outcome at 1 week. Furthermore, ^{1}H-MRS was performed under a single TE condition because of time constraints, precluding the use of varying TEs [29, 40] to eliminate lipid resonances that may overlap with the lactate signals. More accurate separation of lactate and lipids by ^{1}H-MRS may improve the correlation between lactate and APT signals. Third, a recent study showed that MTR asymmetry analysis is self-compensating in subtracting pH effects, and that focusing on the signal changes in amide proton resonance can clearly outline pH deficits [8, 28]. Calculating the APT signal separately from water saturation and magnetization transfer contrast may increase pH sensitivity. Future reperfusion studies using separate APT signal analysis with wide-offset *z*-spectra data points (8–14 ppm) for correction [41, 42] may therefore strengthen our findings. Finally, a 7-T field strength can result in more selective irradiation of amide protons and better spectral resolution than a 3-T field strength [3, 43], limiting the direct translation of our results to imaging at 3-T field strength. Further studies at 3 T are warranted to determine the optimal RF saturation power level for increasing the specificity of the APT effect.

In conclusion, APT-weighted MRI signals demonstrated a significant temporal reversal after reperfusion and were negatively correlated with lactate content. As APT-weighted MRI provides unique information on tissue acidosis and its reversal, it could potentially be incorporated into a multiparametric MR approach to stroke imaging.

Funding This study was supported by a grant (2016-690) from the Asan Institute for Life Sciences, Asan Medical Center, Seoul, Korea.

Compliance with ethical standards

Guarantor The scientific guarantor of this publication is Dong Cheol Woo.

Conflict of interest The authors of this manuscript declare no relationships with any companies whose products or services may be related to the subject matter of the article.

Statistics and biometry We thank Seon Ok Kim for his expertise in statistical analysis.

Informed consent Approval from the institutional animal care committee was obtained.

Ethical approval This study was approved by the Institutional Animal Care and Use Committee of Asan Medical Center.

Methodology
- retrospective
- cross-sectional
- performed at one institution

References

1. Chesler M (2003) Regulation and modulation of pH in the brain. Physiol Rev 83:1183–1221
2. Zhou J, Wilson DA, Sun PZ, Klaus JA, Van Zijl PC (2004) Quantitative description of proton exchange processes between water and endogenous and exogenous agents for WEX, CEST, and APT experiments. Magn Reson Med 51:945–952

3. Zhou JY, Payen JF, Wilson DA, Traystman RJ, van Zijl PC (2003) Using the amide proton signals of intracellular proteins and peptides to detect pH effects in MRI. Nat Med 9:1085–1090
4. Sun PZ, Zhou J, Sun W, Huang J, van Zijl PC (2007) Detection of the ischemic penumbra using pH-weighted MRI. J Cereb Blood Flow Metab 27:1129–1136
5. Zheng Y, Wang XM (2017) Measurement of lactate content and amide proton transfer values in the basal ganglia of a neonatal piglet hypoxic-ischemic brain injury model using MRI. AJNR Am J Neuroradiol 38:827–834
6. Song G, Li C, Luo X et al (2017) Evolution of cerebral ischemia assessed by amide proton transfer-weighted MRI. Front Neurol 8:67
7. Zhou J, van Zijl PC (2011) Defining an acidosis-based ischemic penumbra from pH-weighted MRI. Transl Stroke Res 3:76–83
8. Heo HY, Zhang Y, Burton TM et al (2017) Improving the detection sensitivity of pH-weighted amide proton transfer MRI in acute stroke patients using extrapolated semisolid magnetization transfer reference signals. Magn Reson Med 78:871–880
9. Zong X, Wang P, Kim SG, Jin T (2014) Sensitivity and source of amine-proton exchange and amide-proton transfer magnetic resonance imaging in cerebral ischemia. Magn Reson Med 71:118–132
10. Sun PZ, Murata Y, Lu J, Wang X, Lo EH, Sorensen AG (2008) Relaxation-compensated fast multislice amide proton transfer (APT) imaging of acute ischemic stroke. Magn Reson Med 59: 1175–1182
11. Sun PZ, Benner T, Kumar A, Sorensen AG (2008) Investigation of optimizing and translating pH-sensitive pulsed-chemical exchange saturation transfer (CEST) imaging to a 3T clinical scanner. Magn Reson Med 60:834–841
12. Sun PZ, Benner T, Copen WA, Sorensen AG (2010) Early experience of translating pH-weighted MRI to image human subjects at 3 tesla. Stroke 41:S147–S151
13. Campbell BC, Mitchell PJ, Kleinig TJ et al (2015) Endovascular therapy for ischemic stroke with perfusion-imaging selection. N Engl J Med 372:1009–1018
14. Jokivarsi KT, Hiltunen Y, Tuunanen PI, Kauppinen RA, Grohn OH (2010) Correlating tissue outcome with quantitative multiparametric MRI of acute cerebral ischemia in rats. J Cereb Blood Flow Metab 30:415–427
15. Dani KA, Warach S (2014) Metabolic imaging of ischemic stroke: the present and future. AJNR Am J Neuroradiol 35:S37–S43
16. Kidwell CS, Saver JL, Mattiello J et al (2000) Thrombolytic reversal of acute human cerebral ischemic injury shown by diffusion/perfusion magnetic resonance imaging. Ann Neurol 47:462–469
17. Weiss HR, Grayson J, Liu X, Barsoum S, Shah H, Chi OZ (2013) Cerebral ischemia and reperfusion increases the heterogeneity of local oxygen supply/consumption balance. Stroke 44:2553–2558
18. Tietze A, Blicher J, Mikkelsen IK et al (2014) Assessment of ischemic penumbra in patients with hyperacute stroke using amide proton transfer (APT) chemical exchange saturation transfer (CEST) MRI. NMR Biomed 27:163–174
19. Kilkenny C, Altman DG (2010) Improving bioscience research reporting: ARRIVE-ing at a solution. Lab Anim 44:377–378
20. Isayama K, Pitts LH, Nishimura MC (1991) Evaluation of 2,3,5-triphenyltetrazolium chloride staining to delineate rat brain infarcts. Stroke 22:1394–1398
21. Sun PZ, Farrar CT, Sorensen AG (2007) Correction for artifacts induced by B(0) and B(1) field inhomogeneities in pH-sensitive chemical exchange saturation transfer (CEST) imaging. Magn Reson Med 58:1207–1215
22. Guivel-Scharen V, Sinnwell T, Wolff SD, Balaban RS (1998) Detection of proton chemical exchange between metabolites and water in biological tissues. J Magn Reson 133:36–45
23. Keupp J, Baltes C, Harvey P, van den Brink J (2011) Parallel RF transmission based MRI technique for highly sensitive detection of amide proton transfer in the human brain at 3T. In: Proc Intl Soc Mag Reson Med 19
24. Maes F, Collignon A, Vandermeulen D, Marchal G, Suetens P (1997) Multimodality image registration by maximization of mutual information. IEEE Trans Med Imaging 16:187–198
25. Cox RW (1996) AFNI: software for analysis and visualization of functional magnetic resonance neuroimages. Comput Biomed Res 29:162–173
26. Zhang XY, Wang F, Jin T et al (2017) MR imaging of a novel NOE-mediated magnetization transfer with water in rat brain at 9.4 T. Magn Reson Med 78:588–597
27. Shen Q, Meng X, Fisher M, Sotak CH, Duong TQ (2003) Pixel-by-pixel spatiotemporal progression of focal ischemia derived using quantitative perfusion and diffusion imaging. J Cereb Blood Flow Metab 23:1479–1488
28. Leigh R, Knutsson L, Zhou J, van Zijl PC (2017) Imaging the physiological evolution of the ischemic penumbra in acute ischemic stroke. J Cereb Blood Flow Metab 38:1500–1516
29. Harada K, Honmou O, Liu H, Bando M, Houkin K, Kocsis JD (2007) Magnetic resonance lactate and lipid signals in rat brain after middle cerebral artery occlusion model. Brain Res 1134:206–213
30. Orlowski P, Chappell M, Park CS, Grau V, Payne S (2011) Modelling of pH dynamics in brain cells after stroke. Interface Focus 1:408–416
31. Lee D, Zhao X, Heo H, Zhang Y, Jiang S, Zhou J (2016) Dynamic changes of amide proton transfer (APT) and multi-parametric MR signals in transient focal ischemia in rats. In: Proc 24th Annual Meeting ISMRM Singapore
32. An HY, Ford AL, Chen YS et al (2015) Defining the ischemic penumbra using magnetic resonance oxygen metabolic index. Stroke 46:982–988
33. Pan J, Konstas AA, Bateman B, Ortolano GA, Pile-Spellman J (2007) Reperfusion injury following cerebral ischemia: pathophysiology, MR imaging, and potential therapies. Neuroradiology 49: 93–102
34. Bivard A, Krishnamurthy V, Stanwell P et al (2014) Spectroscopy of reperfused tissue after stroke reveals heightened metabolism in patients with good clinical outcomes. J Cereb Blood Flow Metab 34:1944–1950
35. Wey HY, Desai VR, Duong TQ (2013) A review of current imaging methods used in stroke research. Neurol Res 35:1092–1102
36. Obrenovitch TP (1995) The ischaemic penumbra: twenty years on. Cerebrovasc Brain Metab Rev 7:297–323
37. Thornton JS, Ordidge RJ, Penrice J et al (1998) Temporal and anatomical variations of brain water apparent diffusion coefficient in perinatal cerebral hypoxic-ischemic injury: relationships to cerebral energy metabolism. Magn Reson Med 39:920–927
38. Xue R, Sawada M, Goto S et al (2001) Rapid three-dimensional diffusion MRI facilitates the study of acute stroke in mice. Magn Reson Med 46:183–188
39. Dijkhuizen RM, Knollema S, van der Worp HB et al (1998) Dynamics of cerebral tissue injury and perfusion after temporary hypoxia-ischemia in the rat: evidence for region-specific sensitivity and delayed damage. Stroke 29:695–704
40. Yamasaki F, Takaba J, Ohtaki M et al (2005) Detection and differentiation of lactate and lipids by single-voxel proton MR spectroscopy. Neurosurg Rev 28:267–277
41. Heo HY, Zhang Y, Lee DH, Hong X, Zhou J (2016) Quantitative assessment of amide proton transfer (APT) and nuclear overhauser enhancement (NOE) imaging with extrapolated semi-solid

magnetization transfer reference (EMR) signals: application to a rat glioma model at 4.7 tesla. Magn Reson Med 75:137–149

42. Heo HY, Zhang Y, Jiang S, Lee DH, Zhou J (2016) Quantitative assessment of amide proton transfer (APT) and nuclear overhauser enhancement (NOE) imaging with extrapolated semisolid magnetization transfer reference (EMR) signals: II. Comparison of three EMR models and application to human brain glioma at 3 tesla. Magn Reson Med 75:1630–1639
43. Dula AN, Smith SA, Gore JC (2013) Application of chemical exchange saturation transfer (CEST) MRI for endogenous contrast at 7 tesla. J Neuroimaging 23:526–532